Bibliography

Askeland, D. R., "*The Science and Engineering of Materials*", Stanley Thornes (Publishers) Ltd; 1996.

Atkinson, P. J., "*Variation in Trabecular Structure of Vertebrae with Age*", Calcif Tissue Res 1:24-32; 1967.

Badiei, A., Bottema., M.J. and Fazzalari, N.L., "*Expected and Observed Changes to Architectural Parameters of Trabecular Bone with Aging - A Comparison of Measurement Techniques*", Digital Image Computing: Techniques and Applications, 2005. DICTA ' 05. Proceedings:491 - 497; 2005.

Benhamou, C. L., Lespessailles, E., Jacquet, G., Harba, R., Jennane, R., Loussot, T., Tourliere, D., and Ohley, W., "*Fractal Organization of Trabecular Bone Images on Calcaneus Radiographs*", J Bone Miner Res 9:1909-18; 1994.

Bocchi, L., and Nori, J., "*Shape Analysis of Microcalcifications using Radon Transform*". Med Eng Phys 29:691-8; 2007.

Boskey, A. L., "*Bone Mineralization*". In: S. C. Cowin (ed.), "*Bone Mechanics Handbook*", pp. 5/1 - 5/33: CRC Press; 2001.

Brinckmann, P., Biggemann, M., and Hilweg, D., "*Prediction of the Compressive Strength of Human Lumbar Vertebrae*". Spine 14:606-10; 1989.

Buckland-Wright, J. C., Lynch, J. A., Rymer, J., and Fogelman, I., "*Fractal Signature Analysis of Macroradiographs Measures Trabecular Organization in Lumbar Vertebrae of Postmenopausal Women*". Calcif Tissue Int 54:106-12; 1994.

Caldwell, C. B., Willett, K., Cuncins, A. V., and Hearn, T. C., "*Characterization of Vertebral Strength Using Digital Radiographic Analysis of Bone Structure*". Med Phys 22:611-5; 1995.

Caligiuri, P., Giger, M. L., Favus, M. J., Jia, H., Doi, K., and Dixon, L. B., "*Computerized Radiographic Analysis of Osteoporosis: Preliminary Evaluation*". Radiology 186:471-4; 1993.

Cendre, E., Mitton, D., Roux, J. P., Arlot, M. E., Duboeuf, F., Burt-Pichat, B., Rumelhart, C., Peix, G., and Meunier, P. J., "*High-Resolution Computed Tomography for Architectural Characterization of Human Llumbar Cancellous Bone: Relationships with Histomorphometry and Biomechanics*". Osteoporos Int 10:353-60; 1999.

Chappard, C., Brunet-Imbault, B., Lemineur, G., Giraudeau, B., Basillais, A., Harba, R., and Benhamou, C. L., "*Anisotropy Changes in Post-Menopausal Osteoporosis: Characterization by a New Index Applied to Trabecular Bone Radiographic Images*". Osteoporos Int; 2005.

Chappard, D., Guggenbuhl, P., Legrand, E., Basle, M. F., and Audran, M., "*Texture Analysis of X-Ray Radiographs is Correlated with Bone Histomorphometry*". J Bone Miner Metab 23:24-9; 2005.

Ciarelli, M. J., Goldstein, S. A., Kuhn, J. L., Cody, D. D., and Brown, M. B., "*Evaluation of Orthogonal Mechanical Properties and Density of Human Trabecular Bone from the Major Metaphyseal Regions with Materials Testing and Computed Tomography*". J Orthop Res 9:674-82; 1991.

Ciarelli, T. E., Fyhrie, D. P., Schaffler, M. B., and Goldstein, S. A., "*Variations in Three-Dimensional Cancellous Bone Architecture of the Proximal Femur in Female Hip Fractures and in Controls*". J Bone Miner Res 15:32-40; 2000.

Consensus development conference: "*Prophylaxis and Treatment of Osteoporosis*". Osteoporos Int 1:114-7; 1991.

Cortet, B., and Marchandise, X., "*Bone Microarchitecture and Mechanical Resistance*". Joint Bone Spine 68:297 - 305; 2001.

Cowin, S. C., "*The Relationship Between the Elasticity Tensor and the Fabric Tensor*". Mechanics of Materials 4:137 - 147; 1985.

Cowin, S. C., "*Wolff's Law of Trabecular Architecture at Remodeling Equilibrium*". J Biomech Eng 108:83-8; 1986.

Cowin, S. C., and Turner, C. H., "*On the Relationship Between the Orthotropic Young's Moduli and Fabric*". J Biomech 25:1493-4; 1992.

Cowin, S. C., "*Remarks on the paper entitled 'Fabric and Elastic Principal Directions of Cancellous Bone are Closely Related'*". J Biomech 30:1191-3; 1997.

Cowin, S. C., "*The False Premise in Wolff's Law*". In: S. C. Cowin (ed.), Bone Mechanics Handbook, pp. 30/1 - 30/15. New York: CRC Press; 2001.

Cruz-Orive, L. M., Karlsson, L. M., Larsen, S. E., and Wainschtein, F., "*Characterizing Anisotropy: A New Concept*". Micron and Microscopica Acta 23:75 - 76; 1992.

Currey, J. D., "*Bones - Structure and Mechanics*". Princeton University Press; 2002.

Currey, J. D., "*The Many Adaptations of Bone*". J Biomech 36:1487-95; 2003.

Dalle Carbonare, L., Valenti, M.T., Bertoldo, F., Zanatta, M., Zenari, S., Realdi, G., Lo Cascio, V. and Giannini, S., "*Bone Microarchitecture Evaluated by Histomorphometry*". Micron 36:609-616; 2005.

Dempster, D. W., "*Bone Microarchitecture and Strength*". Osteoporos Int 14 Suppl 5:54-6; 2003.

Dequeker, J., Remans, J., Franssen, R., and Waes, J., "*Ageing Patterns of Trabecular and Cortical Bone and their Relationship*". Calcif Tissue Res 7:23-30; 1971.

Ebbesen, E. N., Thomsen, J. S., Beck-Nielsen, H., Nepper-Rasmussen, H. J., and Mosekilde, L., "*Lumbar Vertebral Body Compressive Strength Evaluated by Dual-Energy X-Ray Absorptiometry, Quantitative Computed Tomography, and Ashing*". Bone 25:713-24; 1999.

Engelke, K., Song, S. M., Gluer, C. C., and Genant, H. K., "*A Digital Model of Trabecular Bone*". J Bone Miner Res 11:480-9; 1996.

Faulkner, K. G., Gluer, C. C., Majumdar, S., Lang, P., Engelke, K., and Genant, H. K., "*Noninvasive Measurements of Bone Mass, Structure, and Strength: Current Methods and Experimental Techniques*". AJR Am J Roentgenol 157:1229-37; 1991.

Faulkner, K. G., and Pocock, N., "*Future Methods in the Assessment of Bone Mass and Structure*". Best Pract Res Clin Rheumatol 15:359-83; 2001.

Fazzalari, N. L., Crisp, D. J., and Vernon-Roberts, B., "*Mathematical Modelling of Trabecular Bone Structure: The Evaluation of Analytical and Quantified Surface to Volume Relationships in the Femoral Head and Iliac Crest*". J Biomech 22:901-10; 1989.

Fazzalari, N. L., Forwood, M. R., Smith, K., Manthey, B. A., and Herreen, P., "*Assessment of Cancellous Bone Quality in Severe Osteoarthrosis: Bone Mineral Density, Mechanics, and Microdamage*". Bone 22:381-8; 1998.

Fazzalari, N. L., Parkinson, I. H., Fogg, Q. A., and Sutton-Smith, P., "*Antero-Postero Differences in Cortical Thickness and Cortical Porosity of T12 to L5 Vertebral Bodies*". Joint Bone Spine 73:293-7; 2006.

Field, A., "*Discovering Statistics Using SPSS*": Sage; 2005.

Fyhrie, D. P., and Schaffler, M. B., "*Failure Mechanisms in Human Vertebral Cancellous Bone*". Bone 15:105-9; 1994.

Galante, J., Rostoker, W., and Ray, R. D., "*Physical Properties of Trabecular Bone*". Calcif Tissue Res 5:236-46; 1970.

Geraets, W. G., Van der Stelt, P. F., Netelenbos, C. J., and Elders, P. J., "*A New Method for Automatic Recognition of the Radiographic Trabecular Pattern*". J Bone Miner Res 5:227-33; 1990.

Geraets, W., and Van der Stelt, P., "*Analysis of the Radiographic Trabecular Pattern*". Pattern Recognition Letters 12:575-581; 1991.

Geraets, W. G., Van der Stelt, P. F., and Elders, P. J., "*The Radiographic Trabecular Bone Pattern During Menopause*". Bone 14:859-64; 1993.

Geraets, W. G., Van der Stelt, P. F., Lips, P., Elders, P. J., Van Ginkel, F. C., and Burger, E. H., "*Orientation of the Trabecular Pattern of the Distal Radius Around the Menopause*". J Biomech 30:363-70; 1997.

Geraets, W. G., "*Comparison of Two Methods for Measuring Orientation*". Bone 23:383-8; 1998.

Geraets, W. G., Van der Stelt, P. F., Lips, P., and Van Ginkel, F. C., "*The Radiographic Trabecular Pattern of Hips in Patients with Hip Fractures and in Elderly Control Subjects*". Bone 22:165-73; 1998.

Geraets, W., van Ruijven, L., Verheij, J., van Eijden, T., and van der Stelt, P., "*A Sensitive Method for Measuring Spatial Orientation in Bone Structures*". Dentomaxillofac Radiol 35:319-25; 2006.

Goulet, R. W., Goldstein, S. A., Ciarelli, M. J., Kuhn, J. L., Brown, M. B., and Feldkamp, L. A. "*The Relationship Between the Structural and Orthogonal Compressive Properties of Trabecular Bone*". J Biomech 27:375-89; 1994.

Gregg, E. W., Kriska, A. M., Salamone, L. M., Roberts, M. M., Anderson, S. J., Ferrell, R. E., Kuller, L. H., and Cauley, J. A., "*The Epidemiology of Quantitative Ultrasound: A Review of the Relationships with Bone Mass, Osteoporosis and Fracture Risk*". Osteoporos Int 7:89-99; 1997.

Gundersen, H. J., and Jensen, E. B., "*Stereological Estimation of the Volume-Weighted Mean Volume of Arbitrary Particles Observed on Random Sections*". Journal of Microscopy 138:127 - 142; 1985.

Gundersen, H. J., Boyce, R. W., Nyengaard, J. R., and Odgaard, A., "*The Conneulor: Unbiased Estimation of Connectivity using Physical Disectors Under Projection*". Bone 14:217-22; 1993.

Hahn, M., Vogel, M., Pompesius-Kempa, M., and Delling, G., "*Trabecular Bone Pattern Factor - A New Parameter for Simple Quantification of Bone Microarchitecture*". Bone 13:327-30; 1992.

Hansson, T., and Roos, B., "*Microcalluses of the Trabeculae in Lumbar Vertebrae and their Relation to the Bone Mineral Content*". Spine 6:375-80; 1981.

Hansson, T. H., Keller, T. S., and Panjabi, M. M., "*A Study of the Compressive Properties of Lumbar Vertebral Trabeculae: Effects of Tissue Characteristics*". Spine 12:56-62; 1987.

Harrigan, T. P., and Mann, R. W., "*Characterization of Microsturctural Anisotropy in Orthotropic Materials Using a Second Rank Tensor*". Journal of Material Science 19:761 - 767; 1984.

Herman, G. T., "*Image Reconstruction from Projections*". New York: Academic Press; 1980.

Hildebrand, T., Laib, A., Muller, R., Dequeker, J., and Ruegsegger, P., "*Direct Three-Dimensional Morphometric Analysis of Human Cancellous Bone: Microstructural Data from Spine, Femur, Iliac Crest, and Calcaneus*". J Bone Miner Res 14:1167-74; 1999.

Hildebrand, T., and Ruegsegger, P., "*A New Method for the Model-Independent Assessment of Thickness in 3D Images*". Journal of Microscopy 185:67-75; 1997.

Hildebrand, T., and Ruegsegger, P., "*Quantification of Bone Microarchitecture with the Structure Model Index*". Comput Methods Biomech Biomed Engin 1:15-23; 1997.

Homminga, J., McCreadie, B. R., Ciarelli, T. E., Weinans, H., Goldstein, S. A., and Huiskes, R., "*Cancellous Bone Mechanical Properties from Normals and Patients with Hip Fractures Differ on the Structure Level, Not on the Bone Hard Tissue Level*". Bone 30:759-64; 2002.

Jee, W. S. S., "*Integrated Bone Tissue Physiology: Anatomy and Physiology*". In: S. C. Cowin (ed.), "*Bone Mechanics Handbook*", Second Edition, pp. 1/1 - 1/68, CRC Press, 2001.

Kabel, J., van Rietbergen, B., Odgaard, A., and Huiskes, R., "*Constitutive Relationships of Fabric, Density, and Elastic Properties in Cancellous Bone Architecture*". Bone 25:481-6; 1999.
Kanatani, K., "*Measurement of Particle Orientation Distribution by a Stereological Method*". Part. Charact. 2:31 - 37; 1985.

Kanis, J. A., Delmas, P., Burckhardt, P., Cooper, C., and Torgerson, D., "*Guidelines for Diagnosis and Management of Osteoporosis*". The European Foundation for Osteoporosis and Bone Disease. Osteoporos Int 7:390-406; 1997.

Kanis, J. A., Johnell, O., Oden, A., Dawson, A., De Laet, C., and Jonsson, B., "*Ten Year Probabilities of Osteoporotic Fractures According to BMD and Diagnostic Thresholds*". Osteoporos Int 12:989-95; 2001.

Kanis, J. A., "*Diagnosis of Osteoporosis and Assessment of Fracture Risk*". Lancet 359:1929-36; 2002.

Kaufman, J. J. S., R. S., “*Noninvasive Measurement of Bone Integrity*”. In: S. C. Cowin (ed.), “*Bone Mechanics Handbook*”, Second Edition, pp. 34/1 – 34/35, CRC Press, 2001.

Keaveny, T. M., and Hayes, W. C., “*A 20-year Perspective on the Mechanical Properties of Trabecular Bone*”. J Biomech Eng 115:534-42; 1993.

Keaveny, T. M., Wachtel, E. F., Guo, X. E., and Hayes, W. C., “*Mechanical Behavior of Damaged Trabecular Bone*”. J Biomech 27:1309-18; 1994.

Keaveny, T. M., Pinilla, T. P., Crawford, R. P., Kopperdahl, D. L., and Lou, A., "*Systematic and Random Errors in Compression Testing of Trabecular Bone*”. J Orthop Res 15:101-10; 1997.

Keaveny, T. M., Wachtel, E. F., and Kopperdahl, D. L., “*Mechanical Behavior of Human Trabecular Bone After Overloading*”. J Orthop Res 17:346-53; 1999.

Keaveny, T. M., Morgan, E. F., Niebur, G. L., and Yeh, O. C., “*Biomechanics of Trabecular Bone*”. Annu Rev Biomed Eng 3:307-33; 2001.

Ketcham, R. A., and Ryan, T. M., “*Quantification and Visualization of Anisotropy in Trabecular Bone*”. Journal of Microscopy 213:158 - 171; 2004.

Kitahara, H., “*Morphological Observations on Trabecular Microfractures in the Lumbar Vertebrae”* (author's transl). Nippon Seikeigeka Gakkai Zasshi 54:449-60; 1980.

Kopperdahl, D. L., Pearlman, J. L., and Keaveny, T. M., “*Biomechanical Consequences of an Isolated Overload on the Human Vertebral Body*”. J Orthop Res 18:685-90; 2000.

Laib, A., and Ruegsegger, P., “*Comparison of Structure Extraction Methods for in vivo Trabecular Bone Measurements*”. Comput Med Imaging Graph 23:69-74; 1999.

Lespessailles, E., Chappard, C., Bonnet, N., and Benhamou, C. L., "*Imaging Techniques for Evaluating Bone Microarchitecture*”. Joint Bone Spine; 2006.

Liu, X., Wang, X., and Niebur, G. L., “*Effects of Damage on the Orthotropic Material Symmetry of Bovine Tibial Trabecular Bone*”. J Biomech 36:1753-9; 2003.

Lorensen, W. E. C., H.E., “*Marching Cubes: A High Resolution 3D Surface Construction Algorithm*”. Proceedings of the 14th annual conference on Computer graphics and interactive techniques:163 - 169; 1987.

Luo, G., Kinney, J. H., Kaufman, J. J., Haupt, D., Chiabrera, A., and Siffert, R. S. “*Relationship Retween Plain Radiographic Patterns and Three-Dimensional Trabecular Architecture in the Human Calcaneus*”. Osteoporos Int 9:339-45; 1999.

Marieb, E. N., “*Human Anatomy and Physiology*”: Benjamin Cummings; 1998.

McCalden, R. W., McGeough, J. A., and Court-Brown, C. M., “*Age-Related Changes in the Compressive Strength of Cancellous Bone. The Relative Importance of Changes in Density and Trabecular Architecture*”. J Bone Joint Surg Am 79:421-7; 1997.

Mosekilde, L., and Viidik, A., “*Correlation Between the Compressive Strength of Iliac and vertebral Trabecular Bone in Normal Individuals*”. Bone 6:291-5; 1985.

Mosekilde, L., “*Normal Vertebral Body Size and Compressive Strength: Relations to Age and to Vertebral and Iliac Trabecular Bone Compressive Strength*”. Bone 7:207-12; 1986.

Mosekilde, L., and Danielsen, C. C., “*Biomechanical Competence of Vertebral Trabecular Bone in Relation tTo Ash Density and Age in Normal Individuals*”. Bone 8:79-85; 1987.

Mosekilde, L., “*Age-Related Changes in Vertebral Trabecular Bone Architecture - Assessed by a New Method”*. Bone 9:247-50; 1988.

Mosekilde, L., “*Sex Differences In Age-Related Loss of Vertebral Trabecular Bone Mass and Structure - Biomechanical Consequences”*. Bone 10:425-32; 1989.

Mosekilde, L., "*Vertebral Structure and Strength In Vivo and In Vitro*". Calcif Tissue Int 53 Suppl 1:S121-5; discussion S125-6; 1993.

Mosekilde, L., Ebbesen, E. N., Tornvig, L., and Thomsen, J. S., "*Trabecular Bone Structure and Strength - Remodelling and Repair*". J Musculoskelet Neuronal Interact 1:25-30; 2000.

Muller, R., Van Campenhout, H., Van Damme, B., Van Der Perre, G., Dequeker, J., Hildebrand, T., and Ruegsegger, P., "*Morphometric Analysis of Human Bone Biopsies: A Quantitative Structural Comparison of Histological Sections and Micro-Computed Tomography*". Bone 23:59-66; 1998.

Nguyen, T. V., Center, J. R., and Eisman, J. A., "*Osteoporosis: Underrated, Underdiagnosed and Undertreated*". Med J Aust 180:S18-22; 2004.

Niebur, G. L., Feldstein, M. J., and Keaveny, T. M., "*Biaxial Failure Behavior of Bovine Tibial Trabecular Bone*". J Biomech Eng 124:699-705; 2002.

Niebur, G. L., Yuen, J. C., Burghardt, A. J., and Keaveny, T. M., "*Sensitivity of Damage Predictions to Tissue Level Yield Properties and Apparent Loading Conditions*". J Biomech 34:699-706; 2001.

Odgaard, A., "*Three-Dimensional Methods for Quantification of Cancellous Bone Architecture*". Bone 20:315-28; 1997.

Odgaard, A., Kabel, J., van Rietbergen, B., Dalstra, M., and Huiskes, R., "*Fabric and Elastic Principal Directions of Cancellous Bone are Closely Related*". J Biomech 30:487-95; 1997.

Odgaard, A., "*Quantification of Cancellous Bone Architecture*". In: S. C. Cowin (ed.), "*Bone Biomechanics Handbook*", Second Edition, 14/1 – 14/19, CRC Press, 2001.

Oh, W., and Lindquist, W. B., "*Image Thresholding by Indicator Kriging*". IEEE Transaction on Pattern Analysis and Machine Intelligence 21:590-602; 1999.

Otsu, N., "*A Threshold Selection Method from Gray-Level Histograms*". IEEE Transactions on Systems, Man, and Cybernetics 9:62 - 66; 1979.

Parfitt, A. M., "*Bone Histomorphometry: Techniques and Interpretation*": CRC Press; 1983.

Parfitt, A., Mathews, C., Villanueva, A., Kleerekoper, M., Frame, B., and Rao, D. "*Relationship Between Surface, Volume and Thickness of Iliac Trabecular Bone in Aging and in Osteoporosis*". Journal of Clinical Investigation 72:1396-1409; 1983.

Parfitt, A. M., Drezner, M. K., Glorieux, F. H., Kanis, J. A., Malluche, H., Meunier, P. J., Ott, S. M., and Recker, R. R., "*Bone Histomorphometry: Standardization of Nomenclature, Symbols, and Units*". Report of the ASBMR Histomorphometry Nomenclature Committee. J Bone Miner Res 2:595-610; 1987.

Pothuaud, L., Van Rietbergen, B., Mosekilde, L., Beuf, O., Levitz, P., Benhamou, C. L., and Majumdar, S., "*Combination of Topological Parameters and Bone Volume Fraction Better Predicts the Mechanical Properties of Trabecular Bone*". J Biomech 35:1091-9; 2002.

Rice, J. C., Cowin, S. C., and Bowman, J. A., "*On the Dependence of the Elasticity and Strength of Cancellous Bone on Apparent Density*". J Biomech 21:155-68; 1988.

Reimann, D. A., Fyhrie, D.P., Fazzalari, N.L., Schaffler, M.B., "*Trabecular Bone Morphometry by Volume Projection*". 38th Annual Meeting, Orthopaedic Research Society, pp. 561. Washington, D.C.; 1992.

Rockoff, S. D., "*Quantitative Microdensitometric X-Ray Analysis of Vertebral Trabecular Bone*". A preliminary report. Radiology 88:794-6; 1967.

Rockoff, S. D., "*Radiographic Trabecular Quantitation of Human Lumbar Vertebrae In Situ. I. Theory and Method for Study of Osteoporosis*". Invest Radiol 2:272-89; 1967.

Rockoff, S. D., "*Techniques of Data Extraction from Radiological Images*". An overview. Invest Radiol 7:206-22; 1972.

Rockoff, S. D., Scandrett, J., and Zacher, R., "*Quantitation of Relevant Image Information: Automated Radiographic Bone Trabecular Characterization*". Radiology 101:435-9; 1971.

Rockoff, S. D., Zettner, A., and Albright, J., "*Radiographic Trabecular Quantitation of Human Lumbar Vertebrae In Situ. II. Relation to Bone Quantity, Strength and Mineral Content (Preliminary Results)*". Invest Radiol 2:339-52; 1967.

Roylance, D., "*Stress-Strain Curves*". Cambridge, MA; 2001.

Ruegsegger, P., "*Imaging of Bone Structure*". In: S. C. Cowin (ed.), "*Bone Mechanics Handbook*", Second Edition, pp. 9/1 – 9/24, CRC Press, 2001.

Ruegsegger, P., Koller, B., and Muller, R., "*A Microtomographic System for the Nondestructive Evaluation of Bone Architecture*". Calcif Tissue Int 58:24-9; 1996.

Russ, J. C. Image Processing Handbook: CRC Press; 2002.

Russ, J. C., and Dehoff, R. T., "*Practical Stereology*". New York: Plenum Publishers; 2000.

Siffert, R. S. L., G. Kaufman, J. J., "*Moire Patterns from Plain Radiographs of Trabecular Bone*". Proceedings of the 17th Annual Conference of the IEEE Engineering in Medicine and Biology Society 1:545 - 546; 1995.

Simpson, E. K., Parkinson, I. H., Manthey, B., and Fazzalari, N. L., "*Intervertebral Disc Disorganization is Related to Trabecular Bone Architecture in the Lumbar Spine*". J Bone Miner Res 16:681-7; 2001.

Singh, M., Nagrath, A. R., and Maini, P. S., "*Changes in Trabecular Pattern of the Upper End of the Femur as an Index of Osteoporosis*". J Bone Joint Surg Am 52:457-67; 1970.

Smit, T. H., Schneider, E., and Odgaard, A., "*Star Length Distribution: A Volume-Based Concept for the Characterization of Structural Anisotropy*". J Microsc 191 (Pt 3):249-57; 1998.

Snyder, B. D., "*Anisotropic Structure-Property Relations for Trabecular Bone*". Bioengineering, pp. 260: Univeristy of Pennsylvania; 1991.

Thomsen, J. S., Ebbesen, E. N., and Mosekilde, L., "*A New Method of Comprehensive Static Histomorphometry Applied on Human Lumbar Vertebral Cancellous Bone*". Bone 27:129-38; 2000.

Thomsen, J. S., Ebbesen, E. N., and Mosekilde, L., "*Predicting Human Vertebral Bone Strength By Vertebral Static Histomorphometry*". Bone 30:502-8; 2002.

Turner, C. H., Cowin, S. C., Rho, J. Y., Ashman, R. B., and Rice, J. C., "*The Fabric Dependence of the Orthotropic Elastic Constants of Cancellous Bone*". J Biomech 23:549-61; 1990.

Turner, C. H. and Burr, D. B., "*Experimental Techniques for Bone Mechanics*". In: S. C. Cowin (ed.), "*Bone Mechanics Handbook*", Second Edition, pp. 7/1 - 7/35, CRC Press, 2001.

Ulrich, D., van Rietbergen, B., Laib, A., and Ruegsegger, P., "*The Ability of Three-Dimensional Structural Indices to Reflect Mechanical Aspects of Trabecular Bone*". Bone 25:55-60; 1999.

van Rietbergen, B. a. H., R., "*Elastic Constants of Cancellous Bone*". In: S. C. Cowin (ed.), "*Bone Mechanics Handbook*", pp. 15/1 - 15/24: CRC Press; 2001.

Vesterby, A., Mosekilde, L., Gundersen, H. J., Melsen, F., Holme, K., and Sorensen, S. "*Biologically Meaningful Determinants of the In Vitro Strength of Lumbar Vertebrae*". Bone 12:219-24; 1991.

Waarsing, J. H., Day, J. S., and Weinans, H., "*Longitudinal Micro-CT Scans to Evaluate Bone Architecture*". J Musculoskelet Neuronal Interact 5:310-2; 2005.

Wang, X., Guyette, J., Liu, X., Roeder, R. K., and Niebur, G. L. "*Axial-Shear Interaction Effects on Microdamage in Bovine Tibial Trabecular Bone*". Eur J Morphol 42:61-70; 2005.

Wang, X., and Niebur, G. L., "*Microdamage Propagation in Trabecular Bone Due to Changes in Loading Mode*". J Biomech 39:781-90; 2006.

Whitehouse, W. J., "*The Quantitative Morphology of Anisotropic Trabecular Bone*". J Microsc 101 Pt 2:153-68; 1974.

WHO Technical Report Series (Prevention and Management of Osteoporosis) -

“*Diagnosis and Assessment*”. In: W. S. G. o. P. a. M. o. Osteoporosis (ed.), WHO Scientific Group on Prevention and Management of Osteoporosis, pp. 53(33): World Health Organization; 2003.

WHO Technical Report Series (Prevention and Management of Osteoporosis) – “*Introduction*”. In: W. S. G. o. P. a. M. o. Osteoporosis (ed.), WHO Scientific Group on Prevention and Management of Osteoporosis, pp. 1(9): World Health Organization; 2003.

WHO Technical Report Series (Prevention and Management of Osteoporosis) – “*Pathogenesis of Osteoporosis and Related Fractures*”. In: W. S. G. o. P. a. M. o. Osteoporosis (ed.), WHO Scientific Group on Prevention and Management of Osteoporosis, pp. 10(21): World Health Organization; 2003.

Wolff, J. D., “*Das Gesetz der Transformation der Knochen*”. Berlin, A. Hirschwald. 1892.

Appendix A

Segmentation of Bone from µCT Imaging

Introduction

Micro-CT (µCT) imaging is fast becoming ubiquitous in morphometric investigations of bone. Part of the seduction of µCT imaging is the ability to represent the original sample as a computerised three-dimensional (3D) model. This may also be one of its disadvantages in that the 3D representation may appear to be an authentic representation but it may be inaccurate. If morphometric analysis is required then the investigator must have confidence that what is designated bone really is bone.

µCT imaging provides a series of two-dimensional (2D) tomographs, which enable accurate reconstruction of the specimen as a voxel-based dataset (Figure A.1 [A]). Each tomograph is equivalent to a histological section, whereby in 2D the bone matrix can be clearly delineated from marrow spaces. Importantly, the series of tomographs enables a 3D representation of the bone to be constructed. It is possible from this voxel-based dataset to measure trabecular dimensions using a sphere-fitting algorithm (7) and to apply other model-independent algorithms for bone structure, such as connectivity density (10), structural model index (8) and degree of anisotropy (10, 18). Datasets derived from µCT imaging provide a comprehensive suite of descriptive parameters for bone structure in 3D as well as measurement of the amount of bone.

A key step in the analysis of µCT datasets is the segmentation of the greyscale tomographs into a bone phase and a marrow phase and at present there are a number of available methods (1, 5, 6, 9, 14, 15) (Figure A.1 [B]). Global thresholding is the most common image segmentation method and usually involves the operator visually determining what greyscale range corresponds to bone. The greatest disadvantage with this method is that the operator usually sets the threshold value for the whole dataset, which may be up to 1000 tomographs, from a single image or only a limited number of images. It is however, impractical to manually inspect every tomograph to make allowance for grey-level differences within a large volume of bone. Automated global thresholding methods implemented in a computer program, such as Otsu's (12), can determine a greyscale threshold value for every image in a volume.

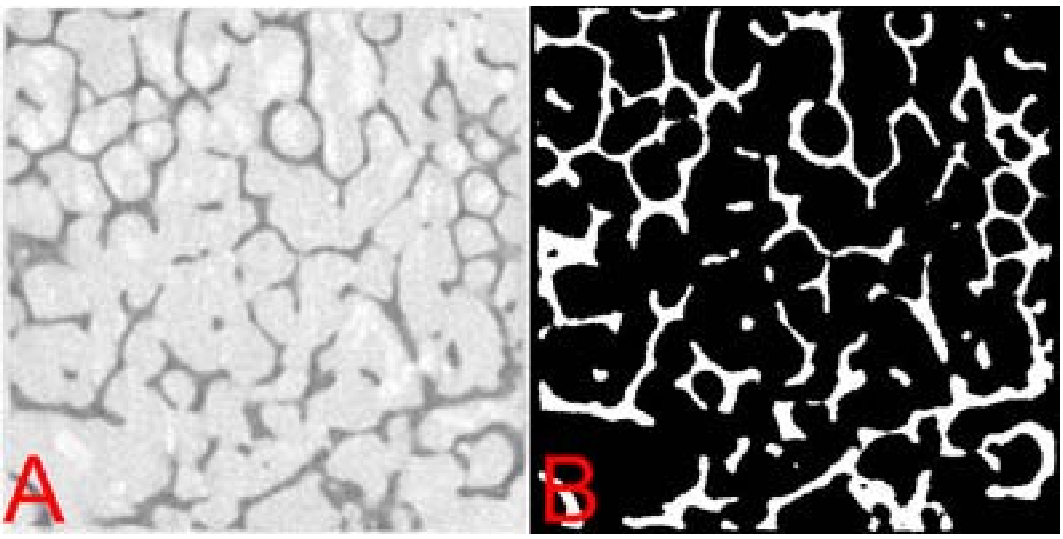

Figure A.1 Example tomograph from a cube of trabecular bone from the centre of the L3 vertebral body. [A] Greyscale tomograph and [B] corresponding segmented binary tomograph.

Local image segmentation techniques are more sensitive to variability within a bone specimen in all three dimensions. The use of local image segmentation has been limited to investigators with specialised computer programming expertise and computer resources greater than that available on desktop computers (11, 16). However, as these high-end computer resources become more accessible, local image segmentation techniques will become more widely used.

Variability in global image segmentation and its effect on morphometric parameters of bone has implications for the biological interpretation of quantitative morphometric analyses. The day to day operations of a laboratory may result in multiple handlers of µCT datasets, which necessitates the establishment of standardised analytical protocols. In this study, the degree to which quantitative morphometric parameters of bone structure are affected by variability in image segmentation will be determined. Recommendations will be made to minimise measurement errors in the quantitative assessment of trabecular bone from µCT imaging.

Materials and Methods

Thoracolumbar vertebral bodies (T12, L1, L3 and L5) were obtained from a 33 year-old female cadaver at autopsy. From each vertebral body, 3 cubes of trabecular bone (10mm x 10mm x 10mm) were cut from the centre of the vertebral body using a diamond blade saw under constant water irrigation.

µCT imaging was performed on all samples (Chapter 2, Section 2.2.3). To determine a 'gold standard' for bone volume fraction (BV/TV) all samples were ashed (Chapter 2, Section 2.2.6) after micro-CT imaging. True bone volume fraction (BV/TV) was calculated as ash-weight (g/cm^3) / bone mineral material density (1.15 g/cm^3) (4).

Segmentation of the greyscale tomographs to discriminate bone matrix from marrow (Figure A.1) on each sample was performed manually by three operators (OP1, OP2 and OP3) using a global threshold technique in which a single grey-level threshold value was selected for each sample. Operator 1 repeated the analysis 3 months after the initial analysis ($OP1_2$). In addition, Otsu's automatic segmentation algorithm was implemented as a custom-written routine in Matlab (The MathWorks). Otsu's algorithm (Otsu) determines a single global grey-level threshold value for each sample (12).

CT analyser software (CTAn) provided by the manufacturer of the µCT system (Skyscan) uses the marching cubes algorithm to generate a surface rendering of the bone (Figure A.2). Using this software, the following three dimensional (3D) model-independent parameters were obtained: bone volume per total volume (BV/TV), trabecular thickness (Tb.Th), trabecular separation (Tb.Sp), trabecular bone pattern factor (TBPf), structural model index (SMI) and degree of anisotropy (DA) (Chapter 2, Section 2.2.3).

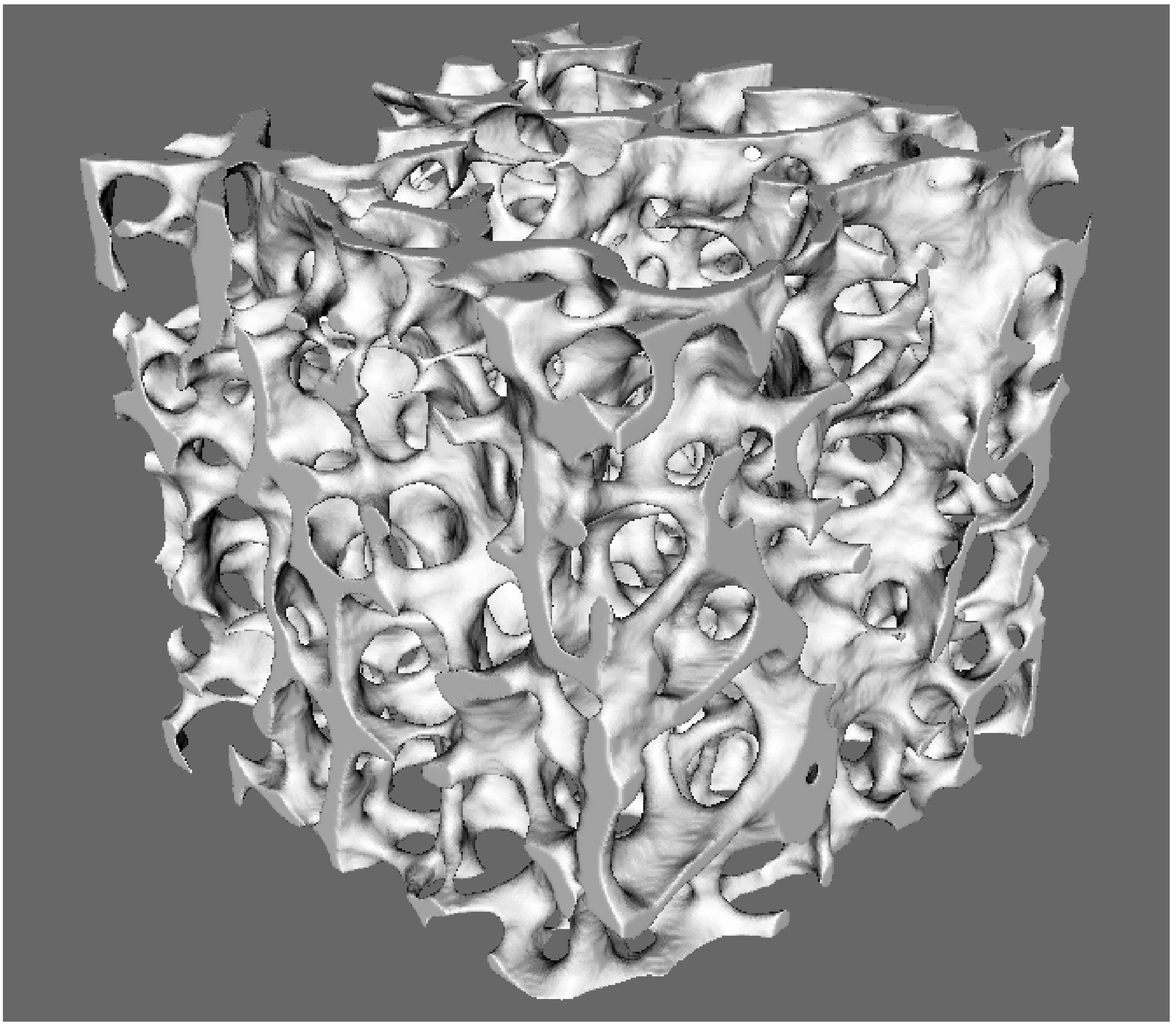

Figure A.2 Three dimensional reconstruction of a cube of vertebral trabecular bone imaged using µCT.

Inter-operator and intra-operator variability for all parameters were calculated as bias and random error (13). Bias is the mean of the differences between operators for the 12 samples, expressed as a percentage of the mean of one of the operators, for each parameter. Random error is standard deviation of the differences between operators for the 12 samples, expressed as a percentage of the mean of one of the operators, for each parameter. While the bias and random error may be positive or negative, only the magnitudes of the differences in morphometric parameters between operators are presented.

Results

Pooled morphometric parameters for the 12 trabecular bone samples, obtained by each operator (OP1, OP2 and OP3) using global thresholding and using Otsu's method for thresholding (Table A.1).

Table A.1 Mean ± standard deviation of the morphometric parameters for the 12 trabecular bone samples obtained by each operator (OP1, OP2 and OP3) using global thresholding and using Otsu's method for thresholding.

	OTSU	OP1	OP2	OP3
GREY LEVEL	186 ± 4	192 ± 5	186 ± 2	179 ± 2
BV/TV (%)	19.0 ± 1.9	21.5 ± 2.1	17.3 ± 2.2	19.5 ± 2.3
Tb.Th (µm)	183 ± 9	196 ± 9	172 ± 12	185 ± 11
Tb.Sp (µm)	728 ± 26	579 ± 109	767 ± 29	703 ± 48
Tb.N (mm^2/mm^3)	1.0 ± 0.1	1.2 ± 0.1	1.0 ± 0.1	1.1 ± 0.1
TBPf (/mm)	4.6 ± 0.9	7.4 ± 2.7	4.2 ± 1.2	4.9 ± 0.9
SMI (-)	1.0 ± 0.2	1.9 ± 0.7	0.9 ± 0.3	1.1 ± 0.2
DA (-)	1.9 ± 0.6	1.9 ± 0.2	1.9 ± 0.2	1.9 ± 0.2

BV/TV calculated from the ash weight of the samples and BV/TV calculated from the µCT datasets, which were segmented by Otsu's method, show excellent concordance ($r^2 = 0.91$, $p<0.0001$) (Figure A.3). Against the 'gold standard' ash weight method, BV/TV using Otsu's method shows a bias of 0.2% and a random error of 1.3%.

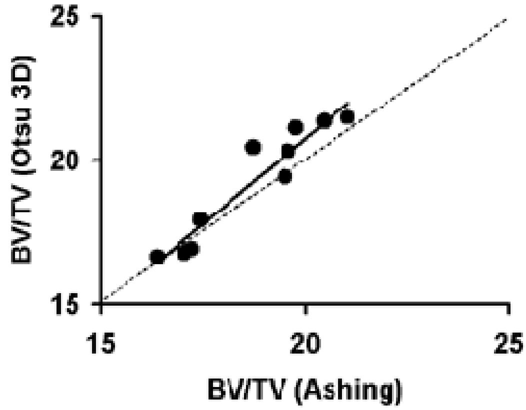

Figure A.3 Scatter plot of BV/TV (Ashing) versus BV/TV (Ostu 3D), which shows excellent concordance between both methods (Y = 1.2X - 2.9, r^2 = 0.91). Broken line represents line of identity.

For grey-level threshold values, bias ranges from 0.1% to 6.9% (Table A.2) and random error ranges from 1.7% to 3.2% (Table A.3).

For BV/TV, bias ranges from 2.3% to 19.6% (Table A.2) and random error ranges from 2.6% to 9.9% (Table A.3). These errors constitute differences in individual measurements between operators in BV/TV of up to 8% (ie. For the sample taken from the right side of L5, BV/TV for OP1=21.4% and BV/TV for OP2=13.7%).

For Tb.Th, bias ranges from 1.3% to 12.2% (Table A.2) and random error ranges from 2.9% to 5.8% (Table A.3). These errors constitute differences between operators in Tb.Th of up to 35µm (ie. For the sample taken from the centre of L5, Tb.Th for OP1=192µm and Tb.Th for OP2=157µm).

For Tb.Sp, bias ranges from 3.4% to 32.4% (Table A.2) and random error ranges from 2.7% to 18.6% (Table A.3). These errors constitute differences between operators in Tb.Sp of up to 306µm (ie. For the sample taken from the right side of L1, Tb.Sp for OP1=475µm and Tb.Sp for OP2=781µm).

For Tb.N, bias ranges from 0.7% to 8.5% (Table A.2) and random error ranges from 2.1% to 5.7% (Table A.3). These errors constitute differences between operators in Tb.N of up to 0.13 mm^{-1} (ie. For the sample taken from the right side of L3, Tb.N for OP1=1.23mm^{-1} and Tb.N for OP2=1.10mm^{-1}).

For TBPf, bias ranges from 6.5% to 59.5% (Table A.2) and random error ranges from 10.1% to 51.1% (Table A.3). These errors constitute differences between operators in TBPf of up to 6.9 mm^{-1} (ie. For the sample taken from the right side of L3, TBPf for OP1=10.9mm^{-1} and TBPf for OP2=4.0mm^{-1}).

For SMI, bias ranges from 9.6% to 81.6% (Table A.2) and random error ranges from 8.5% to 67.9% (Table A.3). These errors constitute differences between operators in SMI of up to 2.1 (ie. For the sample taken from the right side of L3, SMI for OP1=2.95 and SMI for OP2=0.85).

For DA, bias ranges from 0.2% to 1.6% (Table A.2) and random error ranges from 0.8% to 1.8% (Table A.3). These errors constitute differences between operators in DA of up to 0.06 (ie. For the sample taken from the centre of T12, DA for OP1=2.01 and DA for OP2=2.07).

Table A.2 Bias between and within operators (OP1, OP2 and OP3) and Otsu's method for all parameters.

	GREY	BV/TV	Tb.Th	Tb.Sp	Tb.N	TBPf	SMI	DA
OP1 Vs $OP1_2$	0.8	2.4	1.3	6.5	1.2	11.6	13.5	0.2
OP1 Vs OP2	3.2	10.4	5.5	17.6	4.5	49.8	65.6	0.2
OP1 Vs OP3	3.9	11.2	7.3	9.1	4.3	13.7	18.3	1.4
OP2 Vs OP3	6.9	19.6	12.2	32.4	8.5	42.3	50.7	1.6
OP1 Vs Otsu	0.1	2.3	1.4	3.4	0.7	6.5	9.6	0.2
OP2 Vs Otsu	3.1	12.9	7.1	20.4	5.3	59.5	81.6	0.4
OP3 Vs Otsu	4.0	9.2	6.0	5.3	3.6	8.0	10.5	1.2

Table A.3 Random error between and within operators (OP1, OP2 and OP3) and Otsu's method for all parameters.

	GREY	BV/TV	Tb.Th	Tb.Sp	Tb.N	TBPf	SMI	DA
OP1 Vs $OP1_2$	2.6	-2.6	4.5	17.6	3.7	32.5	39.2	1.0
OP1 Vs OP2	2.5	8.7	4.3	13.2	4.2	44.6	57.4	1.2
OP1 Vs OP3	1.7	4.9	3.8	5.2	2.1	13.4	14.1	1.0
OP2 Vs OP3	3.2	9.9	5.8	18.6	5.7	32.3	36.9	1.8
OP1 Vs Otsu	1.9	4.8	2.9	5.6	2.1	10.1	14.5	0.8
OP2 Vs Otsu	2.8	8.6	4.4	14.5	3.7	51.1	67.9	1.4
OP3 Vs Otsu	2.4	5.7	4.0	2.7	3.3	11.4	8.5	1.2

Discussion

Otsu's method for delineating bone matrix from marrow space enables visual representations of the original bone samples to be reconstructed (Figure 3). There is excellent agreement between BV/TV calculated from images binarised by Otsu's method and BV/TV calculated from the ashed samples (Figure 4). Morphometric analysis of the 12 bone samples (Table 1) shows that these samples consist of a network of well-connected trabecular plates with some rod-like structures (SMI = 1.0 ± 0.2) and there is a degree of preferential orientation of the trabeculae (DA = 1.9 ± 0.6).

The variability in the selection of the grey-level threshold value, as measured by bias and random error, is less than 7% between and within operators and Otsu's method (Table 2 and Table 3). These low values indicate that all operators and Otsu's method appear equivalent when delineating between bone matrix and marrow in the trabecularbone samples. However, these small differences constitute large differences when morphometric parameters are calculated. Specifically, up to 8% in BV/TV, 35µm in Tb.Th, 306µm in Tb.Sp and 2.1 in SMI. However, not all parameters show the same sensitivity to changes in grey-level values, such as 0.13mm^{-1} in Tb.N and 0.06 in DA.

Increasingly, morphometric analysis of bones is used to determine the efficacy of therapeutic agents for the prevention of bone loss (2, 3). There is great interest in determining the mechanism by which particular pharmaceutical agents reduce fracture incidence in the absence of measurable changes in the amount of bone (17). The data in this study show that changing an operator during morphometric analysis can introduce errors, which can have a profound effect on biological interpretation. For example, if a pharmaceutical agent was found to increase Tb.Th by 35μm it would be assumed that a catabolic process has occurred, which would be proof of the drug's efficacy. Also, variability of 35μm in Tb.Th within either a control group or a treated group may prevent a real difference between groups from being identified statistically.

These data serve to highlight to users of μCT imaging that subsequent morphometric analysis is highly sensitive to operating parameters. At present, there is no 'correct' method for segmenting bone from marrow in tomographs even though all commonly used segmentation techniques result in visually 'correct' 3D representations of the original bone sample. Ideally, an objective segmentation method should be used that has been validated against a reference sample. However, while objective algorithms do exist there has not been universal adoption of these techniques (14, 16).

Until universally standardised image segmentation techniques have been established it is recommended that a single user perform all morphometric analyses for a particular study. It would also be of value to investigators to perform a limited intra-operator variability study in order to have confidence that a specific user is proficient in the available techniques. All morphometric analyses will have errors associated with methodology but knowledge of the sources and magnitude of these errors will aid investigators in the determining the biological significance of their results.

References

1. Batenburg, K. J., and Sijbers, J. Discrete tomography from micro-CT data: application to the mouse trabecular bone structure. Proceedings of SPIE: Medical Imaging: Physics of Medical Imaging 6142:1325-1335; 2006.
2. Borah, B., Dufresne, T. E., Ritman, E. L., Jorgensen, S. M., Liu, S., Chmielewski, P. A., Phipps, R. J., Zhou, X., Sibonga, J. D., and Turner, R. T. Long-term risedronate treatment normalizes mineralization and continues to preserve trabecular architecture: sequential triple biopsy studies with micro-computed tomography. Bone 39:345-52; 2006.
3. Chesnut, C. H., 3rd, Majumdar, S., Newitt, D. C., Shields, A., Van Pelt, J., Laschansky, E., Azria, M., Kriegman, A., Olson, M., Eriksen, E. F., and Mindeholm, L. Effects of salmon calcitonin on trabecular microarchitecture as determined by magnetic resonance imaging: results from the QUEST study. J Bone Miner Res 20:1548-61; 2005.
4. Dequeker, J., Remans, J., Franssen, R., and Waes, J. Ageing patterns of trabecular and cortical bone and their relationship. Calcif Tissue Res 7:23-30; 1971.
5. Ding, M., Odgaard, A., and Hvid, I. Accuracy of cancellous bone volume fraction measured by micro-CT scanning. Journal of Biomechanics 32:323-326; 1999.
6. Dufresne, T. E. Segmentation techniques for analysis of bone by three-dimensional computed tomographic imaging. Technology and Health Care 6:351-359; 1998.
7. Hildebrand, T., and Ruegsegger, P. A new method for the model-independent assessment of thickness in three-dimensional images. Journal of Microscopy 185:67-75; 1997.
8. Hildebrand, T., and Ruegsegger, P. Quantification of bone microarchitecture with the structure model index. CMBBE 1:15-23; 1997.
9. Hipp, J. A., Jansujwicz, A., Simmons, C. A., and Snyder, B. D. Trabecular bone morphology from micro-magnetic resonance imaging. Journal of Bone and Mineral Research 11:286-297; 1996.
10. Odgaard, A. Three-dimensional methods for quantification of cancellous bone architecture. Bone 20:315-328; 1997.
11. Oh, W., and Lindquist, W. B. Image thresholding by indicator kriging. IEEE Transaction on Pattern Analysis and Machine Intelligence 21:590-602; 1999.
12. Otsu, N. A threshold selection method from gray-scale histogram. IEEE Transactions on Systems Man and Cybernetics 8:62-66; 1978.
13. Parkinson, I. H., and Fazzalari, N. L. Cancellous bone structure analysis using image analysis. Australasian Physical and Engineering Sciences in Medicine 417:64-67; 1994.
14. Rajagopalan, S., Yaszemski, M. J., and Robb, R. Evaluation of thresholding techniques for segmenting scaffold images in tissue engineering. Proceedings of SPIE: Medical Imaging: Image Processing 5370:1456-1465; 2004.
15. Vasilic, B., and Wehrli, F. W. A novel local thresholding algorithm for trabecular bone volume fraction mapping in the limited spatial resolution regime of in vivo MRI. IEEE Transactions on Medical Imaging 24:1574-1585; 2005.
16. Waarsing, J. H., Day, J. S., and Weinans, H. An improved segmentation method for in vivo microCT imaging. Journal of Bone and Mineral Research 19:1640-1650; 2004.
17. Watts, N. B., Geusens, P., Barton, I. P., and Felsenberg, D. Relationship between changes in BMD and nonvertebral fracture incidence associated with risedronate: reduction in risk of nonvertebral fracture is not related to change in BMD. Journal of Bone and Mineral Research 20:2097-2104; 2005.
18. Whitehouse, W. J. The quantitative morphology of anisotropic trabecular bone. Journal of Microscopy 101:153-168; 1974.

Appendix B

Parallel-Plate Model

Introduction

Trabecular bone has a complex three dimensional spatial structure. Histological structural analysis based on tissue sections relies on the parallel-plate model (plate-model) to estimate 3D features. Through estimates of BV/TV and BS/TV, the plate-model enables the calculation of the trabecular architectural parameters, Tb.Th, Tb.Sp and Tb.N (6, 9, 12-14). These model based architectural parameters have been shown to correlate with model-independent measures of architecture (1, 3, 5, 7, 9, 11, 15).

Using dual energy X-ray absorptiometry (DXA), it is possible to estimate bone volume fraction in a non-invasive manner. The PMIL (Chapter 5) allows for measurement of BS/TV from projection based information. Thus, in combination, DXA and PMIL allow for the non-invasive assessment of BV/TV and BS/TV. This presents the opportunity to estimate plate-mode parameters of trabecular architecture in a non-invasive manner.

The aim of this study was to assess the ability of DXA and PMIL to measure plate-model parameters while using μCT model-independent and model-dependent measures as standards.

Materials and Methods

Vertebral bodies from 22 individuals (13 males and 9 females) with an age range 16 – 87 years and median age of 66 years were collected at post-mortem examination. In total, 58 vertebral bodies consisting of 6 T12, 6 L1, 16 L2, 16 L3, 7 L4 and 7 L5 were collected. A cube of trabecular bone was cut from the centrum of each vertebral body (Chapter 2, Section 2.1.1). Cubes were imaged by μCT and processed using standard protocols (Chapter 2, Section 2.2.2). Volumetric bone mineral density (vBMD) of cubes was measured by DXA (Chapter 2, Section 2.2.3) and the bone volume fraction (BV/TV_{DXA}) estimated using the relationship,

$$\frac{BV}{TV} = \frac{vBMD}{\rho_{BONE}},$$

where ρ_{BONE} is the density of the bone tissue and lies between 1 – 2 g/cm^3 (2, 4, 8, 16). A value of 1.15 g/cm^3 (4) was used in this study.

Standard three-dimensional (3D) model-independent measures of trabecular architecture, BV/TV_{3D}, BS/TV_{3D}, $Tb.Th_{3D}$, $Tb.Sp_{3D}$ and $Tb.N_{3D}$ were measured from the datasets (Chapter 2, Section 2.2.2). Using BV/TV_{3D} and BS/TV_{3D}, the plate-model equivalents of the architectural parameters ($Tb.Th_{\mu CT}$, $Tb.Sp_{\mu CT}$ and $Tb.N_{\mu CT}$) were calculated (Chapter 2, Section 2.2.2). DXA based BV/TV (BV/TV_{DXA}) and BS/TV as measured by PMIL (Chapter 5) were used to calculate the non-invasive plate-model equivalents of architectural parameters ($Tb.Th_{PMIL}$, $Tb.Sp_{PMIL}$ and $Tb.N_{PMIL}$).

Statistical differences between group means were tested using analysis of variance (ANOVA) and Student's t-test. Bonferroni's post-hoc test was used to identify groups that achieved significance from ANOVA, while pairwise analyses were carried out to estimate the bias and random error between measures. Bias was defined as the mean of the difference between pair-wise measurements. Random error was defined as the standard deviation of the difference between pair-wise measurements. Regression analyses were used to test relationships between variables. All statistical analyses were performed using a combination of standard routines SPSS (SPSS Inc.) and Matlab (The Mathworks).

Results

Using the µCT 3D model-independent measures of architecture as the referent, no significant differences were observed between males and females for any measured parameter.

BV/TV of L3 trabecular bone cubes was found to be approximately 6% higher than those of L4 trabecular bone cubes (Table B.1). Both T12 and L1 trabecular bone cubes had $Tb.Th_{3D}$ approximately 37µm thinner than those of L2 and L3 trabecular bone cubes (Table B.1).

Table B.1 Mean ± standard deviation of architectural parameters as measured by µCT for the various vertebral levels. Significant differences were identified using Bonferroni post-hoc analyses for $BV/TV_{\mu CT}$ between L3 and L4 (&: p = 0.04) and for $Tb.Th_{3D}$ between T12 and L2 (*: p = 0.04), T12 and L3 (#: p = 0.03), L1 and L2 (%: p = 0.03) and L1 and L3 (^: p = 0.02).

	$BV/TV_{\mu CT}$ (%)	$BS/TV_{\mu CT}$ (mm^2/mm^3)	$Tb.Th_{3D}$ (µm)	$Tb.Sp_{3D}$ (µm)	$Tb.N_{3D}$ (µm)
T12	12.55 ± 3.68	2.36 ± 0.54	180 ± 15*, #	966 ± 132	0.70 ± 0.19
L1	12.49 ± 3.22	2.36 ± 0.48	178 ± 81%,^	970 ± 130	0.70 ± 0.18
L2	14.77 ± 4.36	2.36 ± 0.63	215 ± 27*,%	944 ± 187	0.70 ± 0.22
L3	15.10 ± 5.03&	2.40 ± 0.65	216 ± 25#, ^	926 ± 182	0.70 ± 0.22
L4	9.53 ± 1.09&	1.91 ± 0.28	184 ± 17	1042 ± 132	0.52 ± 0.08
L5	11.26 ± 0.90	2.14 ± 0.31	194 ± 27	989 ± 129	0.59 ± 0.10

3D model-independent measures of thickness and separation were significantly ($p < 0.001$) larger than the thickness and separation measured using the µCT parameter based plate-model (Table B.2). Trabecular number was significantly ($p < 0.001$) smaller for model-independent measurement than for µCT parameter based plate-model (Table B.2).

Table B.2 Mean ± standard deviation of architectural parameters measured by model independent (µCT 3D) and µCT parameter based plate-model (µCT Plate-Model). P value indicates significance of Student's paired t-test.

	µCT 3D	µCT Plate-Model	P
Tb.Th (µm)	202 ± 27	115 ± 15	< 0.001
Tb.Sp (µm)	961 ± 161	807 ± 218	< 0.001
Tb.N (mm^2/mm^3)	0.66 ± 0.19	1.14 ± 0.28	< 0.001

Pair-wise analyses indicated that Tb.Th and Tb.Sp were 40% and 16% smaller for the plate-model than the model-independent measurements, while Tb.N was 62% smaller in model-independent measurements (Table B.3).

The linear relationship between the architectural parameters as measured by the model-independent measurements and µCT parameter based plate-model measurements was computed (Figure B.1). Significant and strong relationships ($r^2 \in [0.78, 0.98]$) were found between all measures.

Table B.3 Results of pair-wise analyses for architectural parameters measured by model independent (µCT 3D) and µCT parameter based plate-model (µCT Plate-Model). The % column is the ratio (BIAS/Referent) x 100, where the Referent is the model-independent measure, and represents the portion of the model-independent measure that the BIAS accounts for.

	BIAS	%	RANDOM ERROR
Tb.Th (µm)	86	43	16
Tb.Sp (µm)	154	16	87
Tb.N (mm^2/mm^3)	0.48	62	0.09

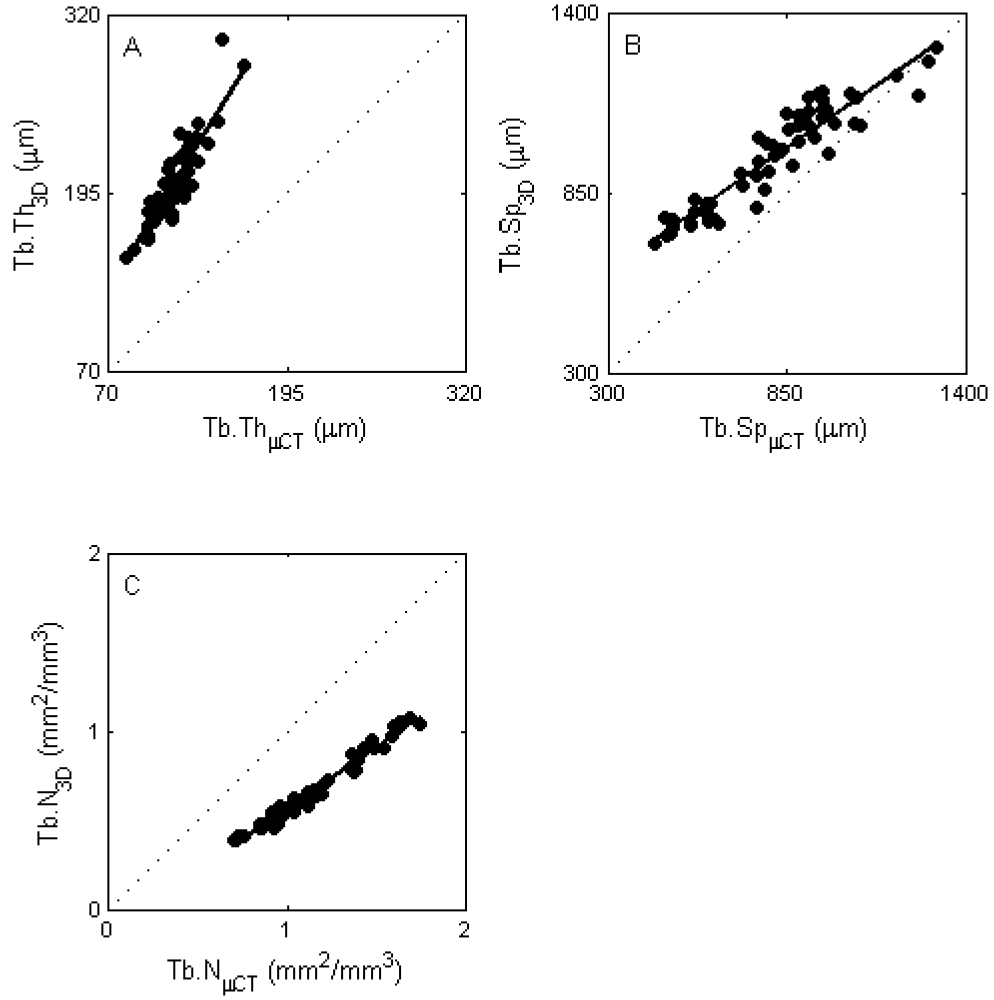

Figure B.1 Linear relationships between model-independent measures and µCT parameter based plate-model measures. [A] $Tb.Th_{3D} = 1.62Tb.Th_{\mu CT} + 14.73$ ($n = 58$, $r^2 = 0.78$ and $p < 0.001$), [B] $Tb.Sp_{3D} = 0.69Tb.Sp_{\mu CT} + 403.21$ ($n = 58$, $r^2 = 0.88$ and $p < 0.001$) and [C] $Tb.N_{3D} = 0.69Tb.N_{\mu CT} – 0.12$ ($n = 58$, $r^2 = 0.97$ and $p < 0.001$). Dotted lines represent lines of identity.

While trabecular thickness was significantly larger in the µCT parameter based plate-model than the DXA/PMIL parameter based plate-model, trabecular separation and number were not found to be significantly different (Table B.4).

Table B.4 Mean ± standard deviation of architectural parameters measured by µCT parameter based plate-model (µCT Plate-Model) and DXA/PMIL parameter base plate-model (DXA/PMIL Plate-Model). P value indicates significance of Student's paired t-test.

	DXA/PMIL Plate-Model	µCT Plate-Model	P
Tb.Th (µm)	55 ± 13	115 ± 15	< 0.001
Tb.Sp (µm)	839 ± 186	807 ± 218	0.14
Tb.N (mm^2/mm^3)	1.16 ± 0.22	1.14 ± 0.28	0.56

Pair-wise analyses indicated that the offset between µCT parameter based plate-model and the DXA/PMIL parameter based plate-model was less that 5% for trabecular separation and number measures (Table B.5).

The linear relationship between the architectural parameters as measured by the µCT parameter based plate-model and the DXA/PMIL parameter based model was computed (Figure B.2). While significant relationships were found between all measures, the linear relationship between trabecular thickness measures was weak (r^2 = 0.09). Much stronger relationships were identified between trabecular separation and number (r^2 = 0.48).

Table B.5 Results of pair-wise analyses for architectural parameters measured by µCT parameter based plate-model (µCT Plate-Model) and DXA/PMIL parameter based plate-model (DXA/PMIL Plate-Model). The % column is the ratio (BIAS/Referent) x 100, where the Referent is the µCT parameter based plate-model measure, and represents the portion of the µCT parameter based plate-model measure that the BIAS accounts for.

	BIAS	%	RANDOM ERROR
Tb.Th (µm)	60	52	23
Tb.Sp (µm)	32	4	165
Tb.N (mm^2/mm^3)	0.02	1	0.21

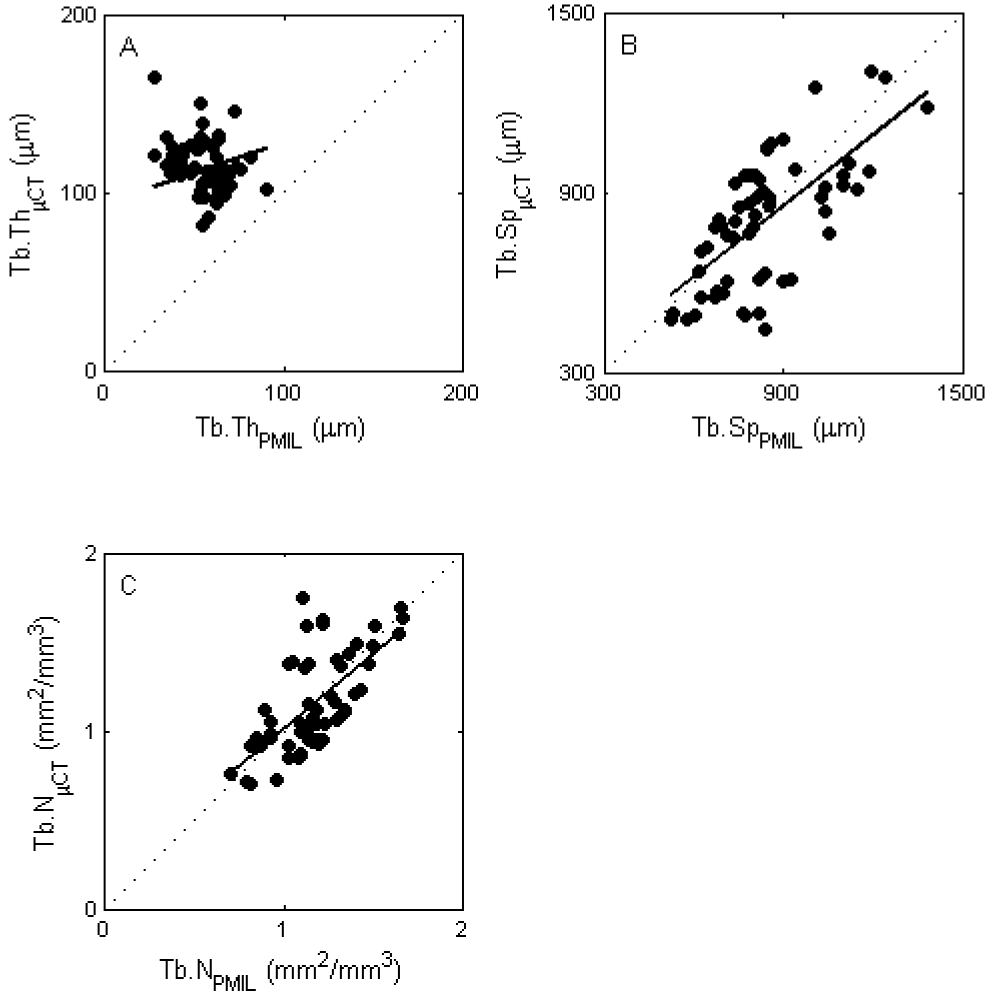

Figure B.2 Linear relationships between µCT parameter based plate-model measures and DXA/PMIL parameter based plate-model measures. [A] $Tb.Th_{\mu CT} = 0.34 Tb.Th_{PMIL} + 134.48$ ($n = 58$, $r^2 = 0.09$ and $p = 0.02$), [B] $Tb.Sp_{\mu CT} = 0.80 Tb.Sp_{PMIL} + 137.46$ ($n = 58$, $r^2 = 0.46$ and $p < 0.001$) and [C] $Tb.N_{\mu CT} = 0.83 Tb.N_{PMIL} + 0.18$ ($n = 58$, $r^2 = 0.46$ and $p < 0.001$). Dotted lines represent line of identity.

Discussion

The parallel-plate model is a tool, which allows estimates of trabecular architectural parameters through knowledge of bone volume fraction and total bone surface. Although this model makes assumptions about the trabecular architecture (Chapter 2), several studies have shown that model based parameters correlate well with model-independent measures of trabecular architecture (7, 9-11). This implies that parallel-plate model estimates are potentially useful clinical tools. If measures of bone volume fraction and total bone surface are made in a non-invasive way, then one can estimate parallel-plate model parameters non-invasively. The aim of this study was to determine if parallel-plate model based measures of trabecular architecture could be estimated using a combination of DXA and PMIL.

Comparisons between µCT model-independent and µCT parameter based models revealed that the parallel-plate model underestimated estimates of trabecular thickness and separation, while overestimating trabecular number. This is likely attributed to deviations of the actual structure from that imposed by the parallel-plate model. Nonetheless, significant correlations were found between model-independent and model-dependent measures of trabecular architecture.

In order to allow a fair comparison, DXA/PMIL model based estimates were tested against µCT parameter based models. In these comparisons, significant relationships were identified between estimates of trabecular separation and number but not thickness. This indicates that non-invasive methodologies can estimate trabecular separation and number as effectively as µCT parameter based models. The modest nature of these relationships is likely the results of poor BV/TV estimation from vBMD measured by DXA (Chapter 7, Section 7.4). Since the relationship between PMIL based BS/TV and µCT based BS/TV is strong (Chapter 5, Section 5.1.4), one would expect that with better estimates of BV/TV, there would be significant improvements in plate-model parameters. This is simply due to the fact that the plate-model estimates of Tb.Th, Tb.Sp and Tb.N are derived from BV/TV and BS/TV alone. No such relationships were identified for trabecular thickness.

While some differences were observed for BV/TV_{3D} and $Tb.Th_{3D}$ between trabecular bone cubes from some vertebral levels, the analyses in this study were pair-wise analyses. As such, the differences found between vertebral levels were not a confounding factor in the study.

In summary, this study has demonstrated the possibility of estimating trabecular architectural measures from non-invasive modalities. While significant work has to be carried out to take such measurements into a clinical setting, this study has demonstrated the possibility and justifies further investigation.

References

1. Cendre, E., Mitton, D., Roux, J. P., Arlot, M. E., Duboeuf, F., Burt-Pichat, B., Rumelhart, C., Peix, G., and Meunier, P. J. High-resolution computed tomography for architectural characterization of human lumbar cancellous bone: relationships with histomorphometry and biomechanics. Osteoporos Int 10*:*353-60; 1999.
2. Currey, J. D. Bones - Structure and Mechanics. Princeton University Press; 2002.
3. Dalle Carbonare, L., Valenti, M.T., Bertoldo, F., Zanatta, M., Zenari, S., Realdi, G., Lo Cascio, V. and Giannini, S. Bone Microarchitecture Evaluated by Histomorphometry. Micron 36*:*609-616; 2005.
4. Dequeker, J., Remans, J., Franssen, R., and Waes, J. Ageing patterns of trabecular and cortical bone and their relationship. Calcif Tissue Res 7*:*23-30; 1971.
5. Engelke, K., Song, S. M., Gluer, C. C., and Genant, H. K. A digital model of trabecular bone. J Bone Miner Res 11*:*480-9; 1996.
6. Fazzalari, N. L., Crisp, D. J., and Vernon-Roberts, B. Mathematical modelling of trabecular bone structure: the evaluation of analytical and quantified surface to volume relationships in the femoral head and iliac crest. J Biomech 22*:*901-10; 1989.
7. Hildebrand, T., Laib, A., Muller, R., Dequeker, J., and Ruegsegger, P. Direct three-dimensional morphometric analysis of human cancellous bone: microstructural data from spine, femur, iliac crest, and calcaneus. J Bone Miner Res 14*:*1167-74; 1999.
8. Keaveny, T. M., Morgan, E. F., Niebur, G. L., and Yeh, O. C. Biomechanics of trabecular bone. Annu Rev Biomed Eng 3*:*307-33; 2001.
9. Laib, A., and Ruegsegger, P. Comparison of structure extraction methods for in vivo trabecular bone measurements. Comput Med Imaging Graph 23*:*69-74; 1999.
10. Lespessailles, E., Chappard, C., Bonnet, N., and Benhamou, C. L. Imaging techniques for evaluating bone microarchitecture. Joint Bone Spine; 2006.
11. Muller, R., Van Campenhout, H., Van Damme, B., Van Der Perre, G., Dequeker, J., Hildebrand, T., and Ruegsegger, P. Morphometric analysis of human bone biopsies: a quantitative structural comparison of histological sections and micro-computed tomography. Bone 23*:*59-66; 1998.
12. Parfitt, A., Mathews, C., Villanueva, A., Kleerekoper, M., Frame, B., and Rao, D. Relationship between surface, volume and thickness of iliac trabecular bone in aging and in osteoporosis. Journal of Clinical Investigation 72*:*1396-1409; 1983.
13. Parfitt, A. M. Bone Histomorphometry: Techniques and Interpretation: CRC Press; 1983.
14. Parfitt, A. M., Drezner, M. K., Glorieux, F. H., Kanis, J. A., Malluche, H., Meunier, P. J., Ott, S. M., and Recker, R. R. Bone histomorphometry: standardization of nomenclature, symbols, and units. Report of the ASBMR Histomorphometry Nomenclature Committee. J Bone Miner Res 2*:*595-610; 1987.
15. Thomsen, J. S., Ebbesen, E. N., and Mosekilde, L. A new method of comprehensive static histomorphometry applied on human lumbar vertebral cancellous bone. Bone 27*:*129-38; 2000.
16. Turner, C. H. and Burr, D. B. Experimental Techniques for Bone Mechanics. In*:* S. C. Cowin (ed.), Bone Mechanics Handbook, Second Edition, pp. 7/1 - 7/35, CRC Press, 2001.